Landes Bioscience www.landesbioscience.com

Supplemental Material to:

Hui Zhang, Fan Wu, Xingwei Wang, Hongwei Du, Xiaochen Wang, Hong Zhang

The two *C. elegans* ATG-16 homologs have partially redundant functions in the basal autophagy pathway

Autophagy 2013; 9(12)
http://dx.doi.org/10.4161/auto.26095

www.landesbioscience.com/journals/autophagy/article/26095

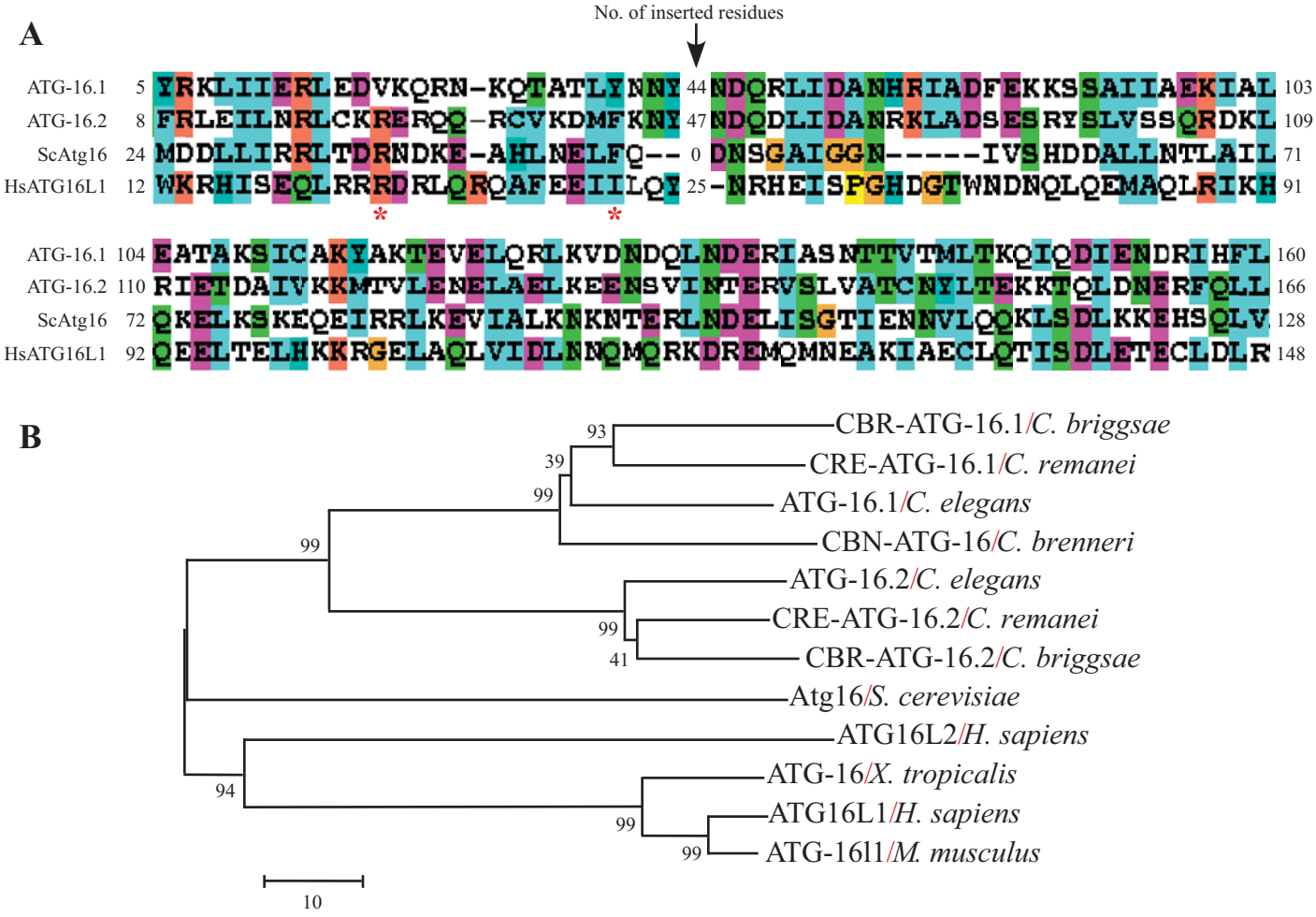

Supplemental Figure S1

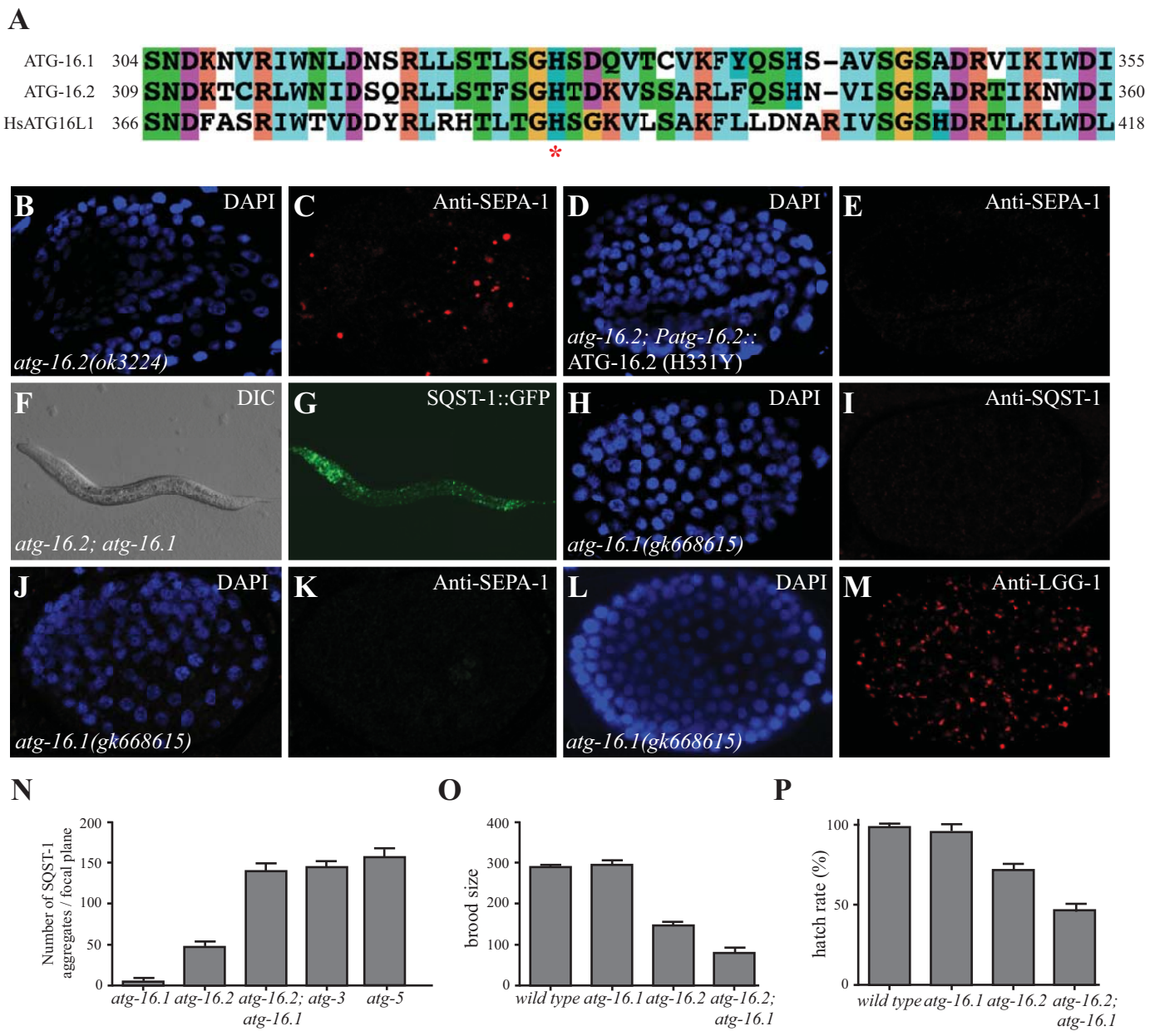

Supplemental Figure S2

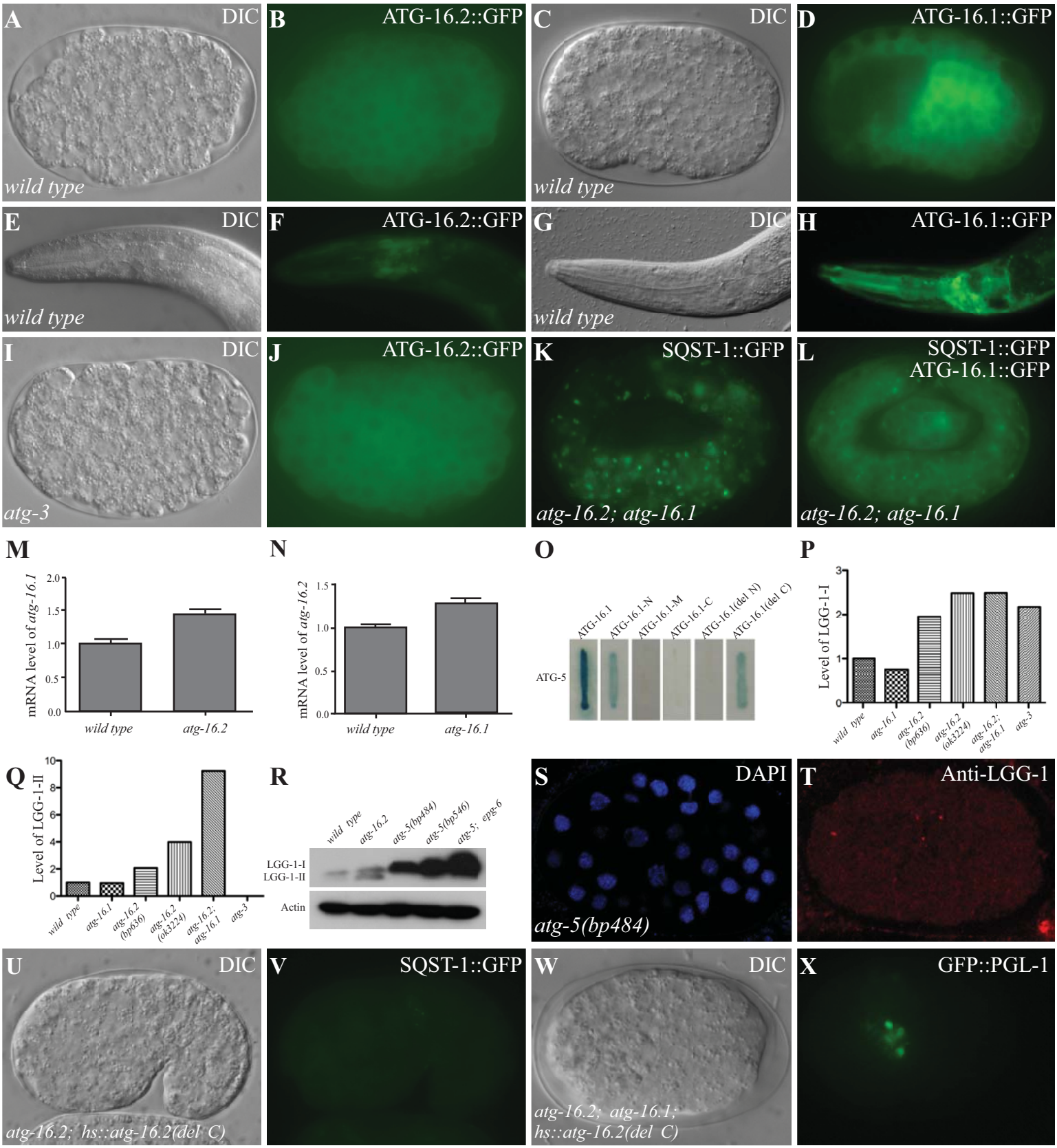

Supplemental Figure S3

Supplemental Figure Legends 12-0684R1

Supplemental figure legends

Figure S1. Sequence alignment and phylogenetic tree of Atg16 family proteins. (**A**) Sequence alignment of Atg16 homologs. The two residues (Arg35 and Phe46) in yeast Atg16 that are critical for interaction with Atg5 are conserved in ATG-16.2 (red asterisks). The number of inserted residues in the linker region is given. Mammalian ATG16L1 and *C. elegans* ATG-16s have the WD repeats at their C termini, which is not shown here. *Hs, H. sapiens*; *Sc, S. cerevisiae*. (**B**) Phylogenetic tree of Atg16 family proteins. MEGA version 4.0 was used to construct a Neighbor-Joining phylogenetic tree. Bootstrap values are shown in percentages at nodes. The 0.1 scale bar represents 10% change.

Figure S2. Role of *atg-16.1* and *atg-16.2* in autophagy-regulated processes. (**A**) The histidine at amino acid 326 in ATG-16.1, which is mutated in *qx57*, is conserved in ATG-16.2 and ATG16L1. (**B and C**) SEPA-1 aggregates are present in an *atg-16.2* mutant embryo at the two-fold stage. (**B**) DAPI image of the embryo shown in (**C**). (**D and E**) Accumulation of SEPA-1 aggregates in *atg-16.2* mutant embryos is rescued by a transgene expressing *Patg-16.2::ATG-16.2(H331Y)*, which contains a histidine to tyrosine mutation at amino acid 331 in ATG-16.2. (**D**). DAPI image of the embryo shown in (**E**). (**F and G**) SQST-1::GFP accumulates into a large number of aggregates in *atg-16.2; atg-16.1* mutant larvae. (**F**) Nomarski image of the embryo shown in (**G**). (**H and I**) SQST-1 aggregates are absent in *atg-16.1(gk668615)* mutant embryos at the ~100 to 200-cell stage. (**H**) DAPI image of the embryo shown in (**I**). (**J and K**) SEPA-1 aggregates

are absent in *atg-16.1(gk668615)* mutant embryos at the comma stage, as in wild-type embryos (**Fig. 1M,N**). (**J**) DAPI image of the embryo shown in (**K**). (**L and M**) *atg-16.1(gk668615)* mutant embryos show a wild-type pattern of LGG-1 puncta (**Fig. 2B,C**) at the ~100 to 200-cell stage. (**L**) DAPI image of the embryo shown in (**M**). (**N**) Average number of SQST-1 aggregates per focal plane in various autophagy mutant embryos at the ~200-cell stage. Error bars represent the standard deviation of five confocal images. (**O**) Brood size in wild type, *atg-16.1, atg-16.2* and *atg-16.2; atg-16.1* animals. (**P**) Hatch rate (% of embryos developed into larvae) in wild type, *atg-16.1, atg-16.2* and *atg-16.2; atg-16.1* animals.

Figure S3. Expression pattern of *atg-16.1* and *atg-16.2* and the requirement of *atg-5* for LGG-1 lipidation. (**A-D**) *atg-16.2::gfp* (**A, B**) and *atg-16.1::gfp* (**C, D**) are ubiquitously expressed in most, if not all, cells in embryos and are localized in the cytoplasm. (**A**) and (**C**). Nomarski images of the animals shown in (**B**) and (**D**), respectively. (**E-H**) Expression of *atg-16.2::gfp* and *atg-16.1::gfp* in the head region. (**E**) and (**G**) Nomarski images of the animals shown in (**F**) and (**H**), respectively. (**I and J**) Expression of *atg-16.2::gfp* remains unchanged in *atg-3* mutants. (**I**) Nomarski image of the embryo shown in (**J**). (**K and L**) A transgene expressing *atg-16.1::gfp* reduces the number of SQST-1 aggregates in *atg-16.2; atg-16.1* double mutants. (**M**) Quantitative real-time PCR analysis reveals that the *atg-16.1* mRNA level in *atg- 16.2(ok3224)* mutants is slightly increased compared to wild-type worms. (**N**) The *atg-16.2* mRNA level is slightly increased in *atg-16.1(qx57)* mutants. (**O**) Interaction between ATG-16.1 and ATG-5 in yeast two-hybrid analysis using an X-gal assay. (**P and Q**) Quantification of levels of LGG-1-I and LGG-1-II shown in Fig. 2A. ImageJ was used to analyze the western blot

image and the level of LGG-1 was normalized to the actin level. (**R**) Western blot analysis reveals that LGG-1-I is greatly elevated but LGG-1-II is absent in *atg-5(bp484), atg-5(bp546)* and *atg-5(bp546); epg-6* mutants. (**S and T**) LGG-1 is diffusely localized in *atg-5(bp484)* mutants at early stage embryos. (**S**). DAPI image of the embryo shown in (**T**). (**U and V**) Accumulation of SQST-1::GFP aggregates in *atg-16.2* mutant embryos (**Fig. 1F**) is rescued by a P*hs*::*atg-16.2(del C)* transgene, in which the C-terminal WD repeats are deleted. (**U**). Nomarski image of the embryo shown in (**V**). (**W and X**) Ectopic accumulation of GFP::PGL-1 granules in *atg-16.2; atg-16.1* mutant embryos (**Fig. 1L**) is rescued by a P*hs*::*atg-16.2(del C)* transgene. (**W**). Nomarski image of the embryo shown in (**X**).